Journal of Catalysis **192,** 432–440 (2000)
doi:10.1006/jcat.2000.2867, available online at http://www.idealibrary.com on IDEAL®

Stability of Highly Dispersed Ni/Al_2O_3 Catalysts: Effects of Pretreatment

Bram W. Hoffer,* A. Dick van Langeveld,*,[1] Jean-Paul Janssens,† Raimond L. C. Bonné,‡ C. Martin Lok,§ and Jacob A. Moulijn*

*Delft ChemTech, Delft University of Technology, Julianalaan 136, 2628 BL Delft, The Netherlands; †Unilever Research, Quarry Road East, Bebington, Wirral L63 3JW, United Kingdom; ‡Synetix, Steintor 9, D-46446 Emmerich, Germany; and §Synetix, P.O. Box 1, Belasis Avenue, Billingham, Cleveland TS 23 1LB, United Kingdom

Received December 9, 1999; revised March 3, 2000; accepted March 5, 2000

Oxidic and reduced and passivated Al_2O_3-supported nickel catalysts with loading up to 19.3 wt% were characterized by temperature-programmed sulfiding (TPS), temperature-programmed reduction (TPR), and X-ray photoelectron spectroscopy. The oxidic catalyst precursors contain a highly disperse nickel species consisting of either an oxidic core and a hydroxide outer layer or a hydroxide as a whole, dependent on the Ni loading. The crystallite size of the active phase varies between 0.4 and 1.6 nm. This high dispersion was maintained during sulfidation. From TPR and TPS, it is inferred that no nickel aluminate is present. During reduction and passivation the crystallite size increases to 1.3–2.5 nm. From TPR of the oxidic catalyst it was concluded that the active phase contained more oxygen than that corresponding to the stoichiometry of NiO since an excess of hydrogen of 20–50% was consumed for the removal of the reactive oxygen species. © 2000 Academic Press

Key Words: **Ni; θ-Al_2O_3; dispersion; pretreatment; sulfidation; reduction; passivation; XPS; TPR; TPS; aluminates.**

INTRODUCTION

Alumina-supported nickel catalysts are extensively used in various oleo- and petrochemical processes. These processes include the de-aromatization of commercial solvents and white oils, hydrogenation of pyrolysis gasoline ("pygas"), olefins, edible oils, and aromatic compounds.

A new generation of hydrotreating catalysts has been developed which combines a high specific nickel surface area and a high reducibility, indicating a high dispersion and a limited, but effective, metal–support interaction (1). They are referred to as HTC catalysts.

The size and morphology of the active phase in the HTC catalysts in the oxidic, reduced, and reduced and passivated state have been determined previously by EXAFS analysis of the higher shells around the Ni atoms (2). In that study it was concluded that, in the oxidic state, Ni cations are present in small NiO_x rafts with predominantly the (111) plane exposed to the gas phase. At low loading (<4.5 wt% Ni), the particles consist of one Ni layer whereas at higher loading the active phase consists of two or three Ni layers. The layer in contact with the Al_2O_3 surface is affected by the support surface and its structure is highly distorted, indicating a strong metal–support interaction. In the reduced state, a monodisperse system was observed, with a limited interaction of the nickel with the support. The crystallites in the reduced and passivated catalyst consist of a Ni kernel of 20–40 metal atoms, covered by a single layer of nickel oxide. For hemispherical particles this corresponds to particles of about 1.6–1.9 nm, respectively.

A highly selective hydrogenation catalyst with limited hydrogenation potential for the conversion of di-olefinic hydrocarbons into mono-olefinic hydrocarbons can be obtained by the partial sulfidation of the nickel (3, 4). This partial sulfidation step is crucial to remove gum and resin precursors in pygas gasoline, while maintaining a high octane number, for which mono-olefins and benzene derivatives in the gasoline are required. In these partially sulfided catalysts, the surface of the Ni particles is poisoned with a limited amount of sulfur atoms, leading to the desired selectivity. The local geometry of S on three low Miller index faces in the outer layer of partial sulfided nickel has been studied extensively with polarization-dependent EXAFS (5–8). Dependent on the low-index surfaces, different high-symmetry adsorption sites for sulfur can be distinguished:

- Two-fold hollow sites on Ni(111)p(2 × 2)–S (5);
- Three-fold hollow sites on Ni(110)c(2 × 2)–S (6);
- Four-fold hollow sites on Ni(100)c(2 × 2)–S (7).

In the present study the sulfidation, carried out with temperature-programmed sulfiding (TPS), is not used to sulfide the nickel oxide precursor partially, but to get a fingerprint of the chemical nature of the nickel species on the catalysts.

Mangnus *et al.* (9) reported differences in the sulfidation behavior of oxidic and reduced nickel catalysts. Their main conclusion was that reduced nickel catalysts sulfide at lower temperatures than their oxidic counterparts. This was

[1] To whom correspondence should be addressed.

0021-9517/00 $35.00

rationalized by a relatively high dissociation rate of chemisorbed H_2S on metallic nickel surfaces as compared to that of their oxidic counterpart (9, 10). The sulfidation mechanism of oxidic nickel catalysts by H_2S occurs by O–S exchange, in accord with results of Arnoldy *et al.* (11).

A problem which is usually encountered in γ-Al_2O_3-supported nickel catalysts is that Ni aluminates are formed due to the incorporation of nickel ions in the surface layers of the support during the impregnation step and/or calcination of the catalysts (12–14). Even in the sulfidation of γ-Al_2O_3-supported nickel catalysts, migration of the Ni species into the support may occur, thus forming nickel aluminate (15). Although the aluminates reflect a stabilizing effect on the nickel particulates, their occurrence is undesired since they are catalytically inactive and, hence, decrease the efficient use of the valuable metal (15, 16).

The present work describes the characterization of oxidic and reduced and passivated nickel catalysts by temperature-programmed reduction (TPR), temperature-programmed sulfiding (TPS), and X-ray photoelectron spectroscopy (XPS). As such, it is complementary to the EXAFS analysis of Shido and co-workers (2). The objective of the characterization is to obtain insight into the chemical nature of the active phase and its crystallite size after various pretreatment conditions. The influence of reduction and sulfidation on the dispersion of the active phase has been investigated.

METHODS

Catalysts

All catalysts were supplied by Synetix and prepared by pore volume impregnation of a transition alumina support, followed by drying and calcination. Optionally, reduction and passivation were applied. The HTC 100–500 series are commercial samples whereas the catalysts containing 1.9 and 4.5 wt% nickel were prepared at the laboratory scale for the quantitative XPS analysis of the catalysts. The nickel content was determined by ICP-AAS.

The nickel surface area of the reduced catalyst was evaluated from static H_2-chemisorption by extrapolation of the amount of reversibly and irreversibly adsorbed H_2 to zero pressure. The catalysts were reduced at 525 K in a pure hydrogen stream for 2 h. The nickel surface area was calculated, under the assumption that a single Ni(111) surface atom chemisorbs one hydrogen atom and that one Ni atom occupies 0.0645 nm^2. Table 1 summarizes the characteristics of the oxidic ("Ox") and the reduced and passivated ("RP") catalysts. The reduced catalysts were passivated in a nitrogen-diluted oxygen gas stream. To establish homogeneous sampling for all experiments and to avoid mass- and heat-transfer limitations in the temperature-programmed reactions, the catalyst extrudates were crushed and sieved, and the particle size fraction between 63 and 150 μm was used.

TABLE 1

Characteristics of the Catalysts Investigated

	Ni (wt%)	BET S.A. ($m^2\ g^{-1}$)	S.A.$_{Ni}$ ($m^2\ g_{Ni}^{-1}$)
HTC 1.9 Ox	1.9	118	170
HTC 4.5 Ox	4.5	124	193
HTC 100 Ox	8.0	130	161
HTC 200 Ox	13.2	126	146
HTC 400 Ox	15.3	125	165
HTC 500 Ox	19.3	138	167
HTC 100 RP	9.4	106	137
HTC 200 RP	13.0	126	157
HTC 400 RP	15.5	110	140
HTC 500 RP	19.0	117	141

Note. S.A. is the BET surface area as determined by N_2 physisorption. S.A.$_{Ni}$ is the nickel surface area based on static hydrogen chemisorption.

Temperature-Programmed Reduction and Sulfiding

The chemical nature of the oxidic and the RP samples was studied by reduction and sulfidation in an atmospheric plug-flow reactor. Depending on the metal loading, the weight of the catalyst sample was varied between 50 and 100 mg. After introduction into the reactor, the catalyst was purged with Ar for 0.5 h. Next, the gas flow was switched to the reactant gas. After the system was stabilized, the sample was heated at a rate of 0.167 K s^{-1}. For TPR, the reactant gas consisted of 22 μmol of H_2 s^{-1} and 11 μmol of Ar s^{-1}. TPS was done in a flow of 0.8 μmol of H_2S s^{-1}, 7.0 μmol of H_2 s^{-1}, and 20.2 μmol of Ar s^{-1}.

In the reactor effluent, H_2S consumption/production was monitored with an UV spectrometer tuned at 205 nm, while the hydrogen consumption was monitored with a thermal conductivity detector (TCD). The production of hydrocarbons, which can be attributed to the hydrogenation of carbonaceous deposits, was monitored with a flame ionization detector (FID). A detailed description of the TPR and TPS apparatus is given by Arnoldy *et al.* (11).

X-ray Photoelectron Spectroscopy

XPS spectra of the oxidic, the RP, and sulfided nickel catalysts were measured in a Perkin–Elmer PHI 5400 ESCA system equipped with a hemispherical analyzer. Mg $K\alpha$ radiation was used for sample excitation. Calibration of the binding energies of the (Ni $2p_{3/2}$) emission line was done by using the (Al $2p$) line of the support at 74.2 eV as the internal reference. In the quantitative analysis of the particle size, the intensity ratio (Ni $3s$) and the (Al $2s$) emission

line was applied. The inelastic mean free path of the (Ni 3*s*) electrons was evaluated from the XPS-cat program, kindly supplied by Gijzeman (17).

The sulfided samples were prepared by sulfidation to 623 K in the gas mixture mentioned above, followed by cooling to room temperature in a flow of the reactant mixture.

RESULTS

TPR

TPR profiles of the oxidic nickel catalysts are collected in Fig. 1. The HTC 100 and HTC 200 catalysts show a broad hydrogen consumption between 500 and 850 K. The HTC 400 and the HTC 500 catalysts show an additional hydrogen consumption in the temperature region from 400 up to 500 K and a sharp hydrogen consumption at approximately 540 K. Both phenomena are less well developed in the TPR profiles of the HTC 100 and HTC 200 catalysts. In the main hydrogen consumption peak, all catalysts show two hydrogen consumptions, peaking at about 615 and 670 K. No measurable hydrogen consumption is observed in the temperature region from 1000 up to 1273 K.

The integrated hydrogen consumption data have been quantified, collected in Table 2 and represent the amount of reactive oxygen in the nickel oxide species. These results clearly show that excess oxygen, which varies from 20 up to 50% is present in the oxidic nickel phase.

TPR profiles of the RP catalysts are collected in Fig. 2. For all samples, the main hydrogen consumption occurs in a well-defined peak with a maximum at 540–560 K. For the HTC 100 and the HTC 200 catalysts an additional hydrogen consumption, peaking at 675 K, can be observed. The integrated hydrogen consumption has been quantified and normalized to the nickel content of the various reduced and passivated catalysts. In the evaluation and the calculation of the proportion of reduced nickel, defined as the "reduction degree," the stoichiometry of the nickel oxide in the reduced and passivated catalyst is assumed to be NiO. These data are summarized in Table 2 and show that the reduction degree of the reduced and passivated catalysts is in the range of 28–40%. This range is slightly higher than the reduction degree of the HTC catalysts determined using TGA.

TABLE 2

Results of the Quantitative TPR Analysis of the Oxidic and Reduced and Passivated Ni/Al_2O_3 Catalysts

Catalyst	H_2/Ni (Ox) (mol/mol)	Reduction degree of RP catalysts (%)[a]	
		TPR	TGA
HTC 100	1.3	39	24
HTC 200	1.4	28	23
HTC 400	1.2	40	36
HTC 500	1.5	35	30

[a] Based on NiO stoichiometry.

TPS

Figure 3 shows the TPS profiles of the oxidic nickel catalysts. From quantitative TPS, which is possible since

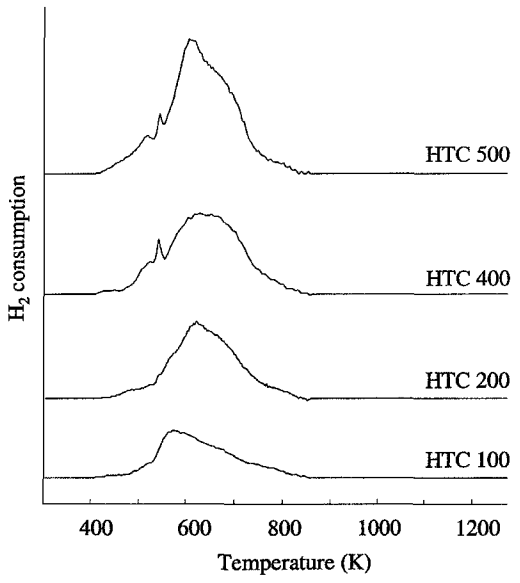

FIG. 1. TPR profiles of the oxidic catalysts. All profiles are normalized to 100 mg of catalyst sample.

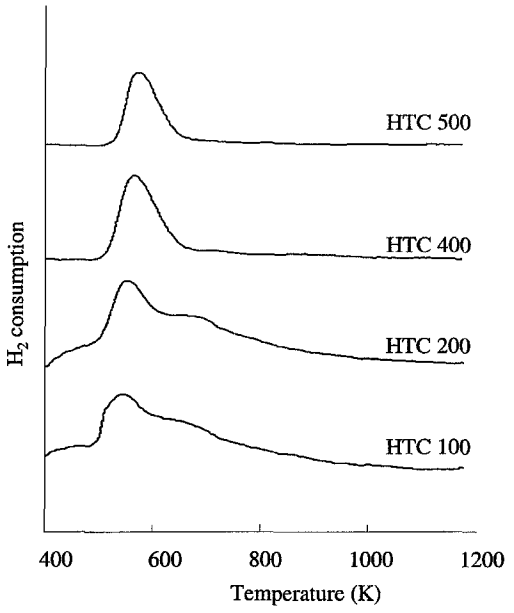

FIG. 2. TPR profiles of the reduced and passivated nickel catalysts. All TPR profiles are normalized to 100 mg of catalyst sample.

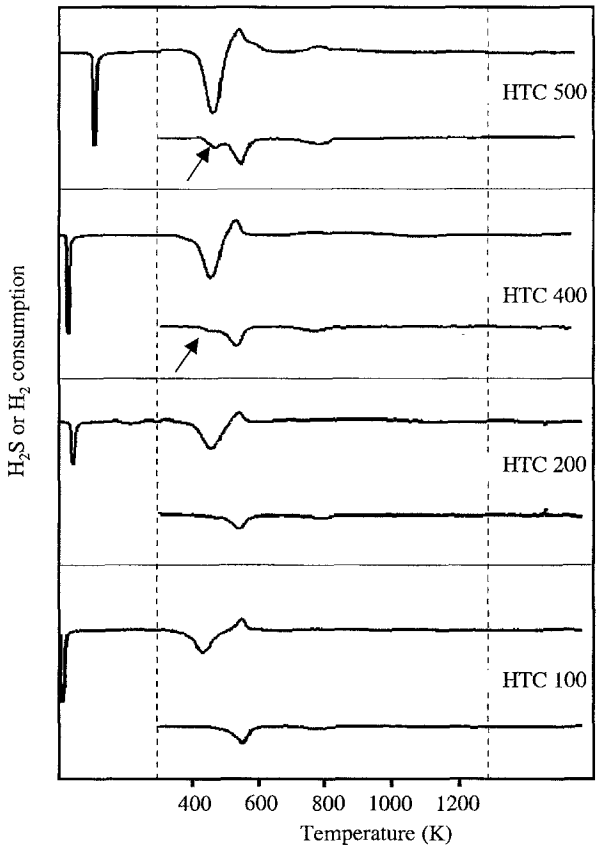

FIG. 3. TPS profiles of the oxidic nickel catalysts (upper curve is the UV signal which represents the H_2S consumption/production; lower curve is the TCD signal representing the H_2 consumption). All TPS profiles are normalized to 100 mg of catalyst sample. The arrow indicates H_2 consumption for the HTC 400 and HTC 500 simultaneously with H_2S consumption.

sublimation of elemental sulfur from the samples was not observed, the amount of sulfur consumed by the oxidic nickel catalyst precursor can be determined in the various stages of sulfidation. Table 3 summarizes these quantitative data for the hydrogen and H_2S uptake and production, normalized to 0.1 g of catalyst. The sulfur-to-nickel molar ratios at 623 and 1273 K are also given in this table.

In the TPS profiles of all samples an H_2S consumption was observed during the isothermal stage at room temperature ("region 1"). After the start of the temperature program, slightly above room temperature ("region 2"), a small amount of H_2S was produced without a simultaneously occurring hydrogen consumption.

In the temperature region from 350 up to 500 K ("region 3"), a major H_2S consumption can be seen for all catalysts. For the HTC 100 and HTC 200 catalysts no significant change in H_2 concentration is observed in this region. However, the HTC 400 and HTC 500 catalysts do show H_2 consumption (indicated by an arrow) simultaneously with the H_2S consumption. At temperatures from 500 up to 600 K ("region 4"), all profiles show a simultaneous H_2 consumption and H_2S production (in stoichiometric amounts), which increase with increasing metal loading. In the temperature region from 700 up to 1000 K, all profiles also show a minor H_2 consumption and H_2S production at about 790 K. During the isothermal sulfidation at 1273 K no H_2S consumption or production was observed.

XPS

Binding energy regimes containing the (Ni $2p_{1/2}$) and (Ni $2p_{3/2}$) emission lines of the oxidic nickel catalyst are presented in Fig. 4. The position of the (Ni $2p_{3/2}$) line varies between 856.1 and 856.4 eV. For all catalysts, the (Ni $2p_{1/2}$) emission lines are found at a 17.8-eV higher binding energy as compared to the (Ni $2p_{3/2}$) line. For both (Ni $2p_{1/2}$) and the (Ni $2p_{3/2}$) emission lines a shake up satellite can be seen at about 6.2- and 6.0-eV higher binding energy values, respectively.

Figure 5 shows the (Ni $3s$)/(Al $2s$) intensity ratios for the oxidic catalysts and their sulfided counterparts as a function of the metal loading in the oxidic precursor. This figure contains the data of two additional low-loading samples containing only 1.9 and 4.5 wt% Ni. As can be seen, for the

TABLE 3

H_2S and H_2 Consumptions and Productions in the Various Regimes[a] (μmol/100 mg_{cat}) and the Corresponding Sulfur-to-Nickel Ratios Obtained from the Quantitative TPS of the Oxides (mol/mol) (Positive Values Indicate Production and Negative Values Consumption of H_2 and H_2S)

	Region 1		Region 2		Region 3		Region 4		Total uptake (673 K)		S/Ni	S/Ni
	H_2	H_2S	H_2	H_2S	H_2	H_2S	H_2	H_2S	H_2	H_2S	(623 K)	(1273 K)
HTC 100		−53		2	0	−132	0	49	0	−134	0.77	0.69
HTC 200		−47		6	−6	−255	−47	39	−53	−257	0.72	0.65
HTC 400		−66		2	−16	−358	−80	70	−96	−352	0.81	0.74
HTC 500		−102		31	−45	−446	−152	185	−197		0.70	0.60

[a] The exact boundaries of the regimes differ slightly for the various catalysts since they are determined by the crossover point of the signals and the baseline in the various plots.

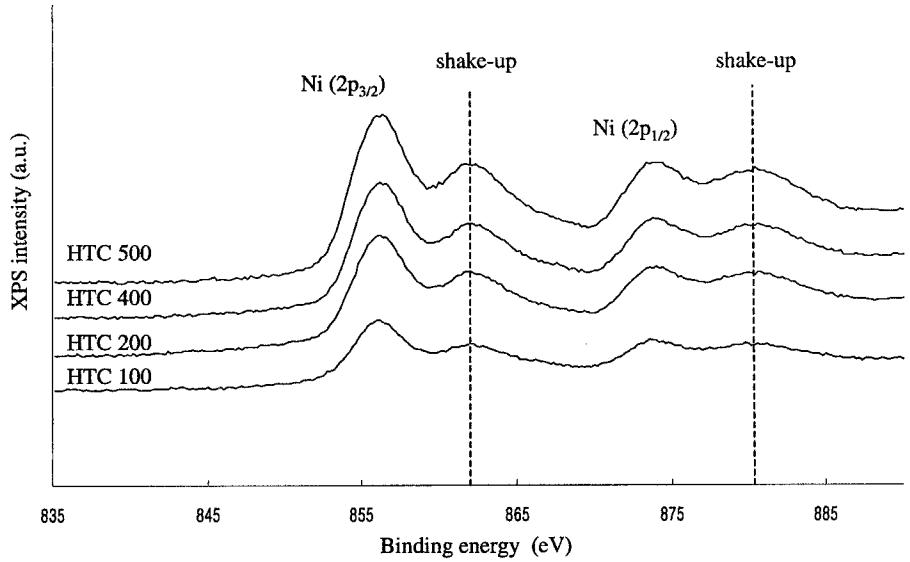

FIG. 4. XPS spectra of the (Ni 2*p*) emission lines of the oxidic catalyst.

three catalysts with the lowest nickel loading a linear correlation exists between the (Ni 3*s*)/(Al 2*s*) intensity ratio and the Ni loading, suggesting an atomic dispersion for these samples. At higher Ni loading the intensity ratio deviates increasingly from the extrapolated straight line.

In Fig. 6 the (Ni 3*s*)/(Al 2*s*) intensity ratios of the RP catalysts and their sulfided counterparts are plotted as a function of the metal loading in the oxidic precursor. The straight line that represents the correlation found for the three oxidic catalysts with the lowest loading is also shown in this figure. All ratios deviate increasingly from the linear correlation with increasing nickel loading and deviate more from it than the oxidic catalysts (Fig. 5).

DISCUSSION

The nature of the nickel phase can be inferred from the XPS emission lines. Basically, one can expect NiO, Ni_2O_3, or $Ni(OH)_2$ to be present. Since the position of the (Ni $2p_{3/2}$) line in the oxidic catalysts is found at 856.1–856.4 eV, the

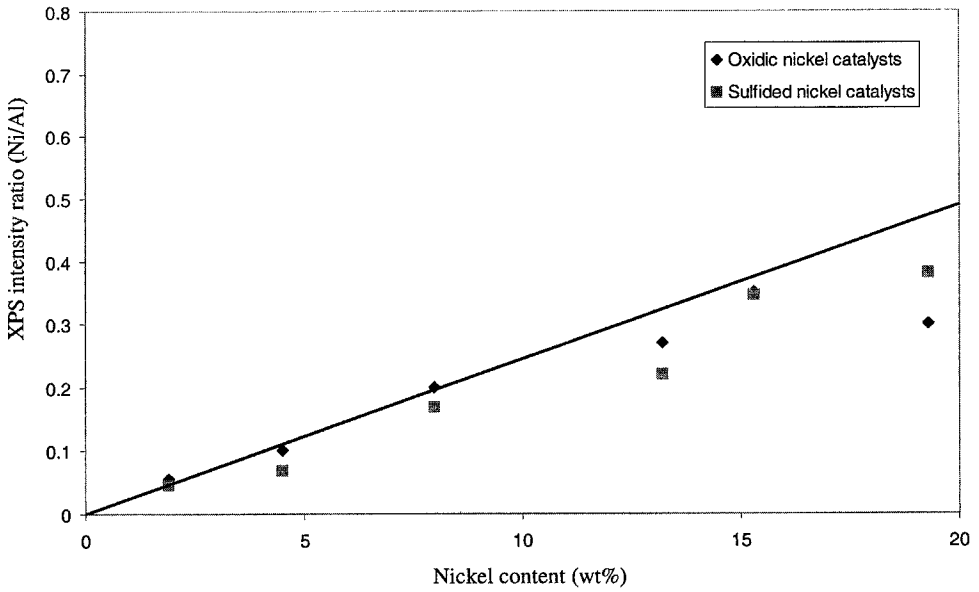

FIG. 5. XPS intensities ratio (Ni 3*s*)/(Al 2*s*) of the oxidic catalyst and its sulfided counterpart as a function of the nickel loading; the straight line is the best fit linear correlation at low metal loading of the oxidic precursor.

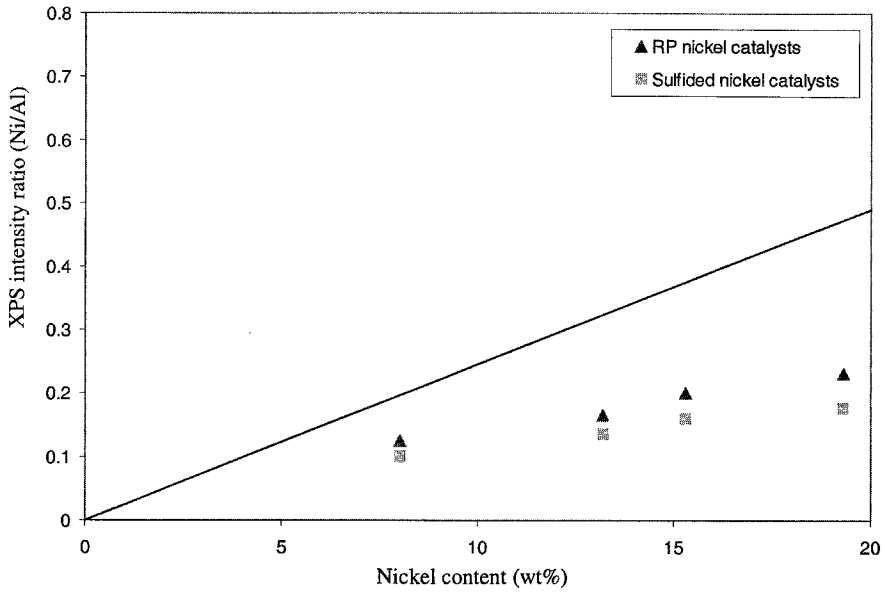

FIG. 6. The (Ni 3*s*)/(Al 2*s*) intensity ratio of the reduced and passivated catalyst precursor and its sulfided counterpart as a function of the nickel loading. The straight line is the best fit linear correlation at low metal loading of the oxidic precursor.

presence of NiO is highly unlikely because the ($2p_{3/2}$) emission line is located at 853.3 eV (18–23). Also, the shape of the ($2p_{3/2}$) line differs from that of NiO, and its distance from the ($2p_{1/2}$) line, 17.8 eV, does not correspond to that of NiO (18.4 eV). Hence, the nickel must be present as Ni_2O_3 or as a hydroxide. Since the binding energy of Ni_2O_3 is found at about the same value as that for $Ni(OH)_2$ (19–21), its position cannot be used to discriminate both options. However, for all catalysts investigated, the shapes of the L_3VV Auger line observed at 411.6 eV and the $L_3M_{23}V$ Auger transition at 480.6 eV show a strong similarity to that of $Ni(OH)_2$ (20), and the differences in kinetic energy between these Auger peaks are 79.8 and 69.7 eV for Ni_2O_3 and $Ni(OH)_2$, respectively, where the HTC catalysts show a ΔE_{kin} of ca. 69 eV. This conclusion is in accordance with the literature, where Ni_2O_3 is reported to be unstable under the conditions of relevance (20, 21). The apparent controversy with the results of Shido *et al.* (2), who conclude that the particles consist of NiO_x, may be understood as follows. At low loading, the active phase consists of a single, (111)-oriented monolayer of hydroxide. Due to the interaction with the support, the Ni–Ni distances in this layer are slightly compressed to a value very similar to that of NiO. At higher loading, multilayer growth of the active phase occurs. In such a case, the first layer on the support could indeed be NiO, the outer layer being a hydroxide, although it cannot be excluded from the current results that the first layer also is a hydroxide. Since, however, EXAFS indicates the presence of a Ni–Ni(o2) shell at about 0.417 nm, which is indicative of the presence of NiO, it is suggested that the core of the particle indeed consist of an oxide. This is in accordance with the fact that XPS is a surface-sensitive technique, whereas EXAFS analyzes the particulates as a whole. As it seems, the relative contribution of the oxidic core of the particulates is too small to be observed by XPS. $Ni(OH)_2$ has the CdI_2 structure consisting of hexagonal closed-packed oxygen anions of which the (111) planes have a slightly larger Ni–Ni distance (0.312 nm) as compared to that found by Shido and co-workers for the oxide (0.296–0.300 nm). This allows a gradual transformation between both structures in the same particle. The fact that the nickel phase is a hydroxide and/or an oxide does not affect the quantitative hydrogen consumption in the TPR. For a bulk oxide, one H_2 molecule would react with a single oxygen anion whereas for a bulk hydroxide one H_2 molecule is needed to react with two OH groups to produce two H_2O molecules. Quantitative TPR on the oxidic catalysts reveals that the amount of reactive oxygen per nickel atom varies between 1.2 and 1.5, depending on the nickel loading. The excess oxygen, 20–50%, can be correlated for instance to OH groups bonded on edge and corner Ni ions in the surface of the highly dispersed "oxidic" crystallites. EXAFS analysis on this series of catalysts performed by Shido *et al.* (2) showed that all Ni cations on the oxidic catalysts are surrounded by six oxygen atoms, supporting our conclusion that there is an excess of oxygen anions.

The reduction degree of the RP catalysts, determined by quantitative TPR, is around 30% (Table 2). This range is comparable to that determined by TGA.

The XPS spectra of the RP catalysts are almost identical to those of the oxidic catalyst, which is also the case for the sulfided RP and the sulfided oxidic catalysts. As

can be expected, passivation leads to mild oxidation of the outer surface of the metallic nickel crystallites, in accord and with the EXAFS data of Shido *et al.* (2). Apparently, the contribution of metallic nickel in the XPS spectra is small due to its attenuation by the oxidic surface layer, induction by the oxide, and the relatively small amount of metallic nickel present in the core of the particle, as can be expected for the highly dispersed nickel. The kinetic energy of the (Ni 3*s*) line (1143 eV) corresponds to an inelastic mean free path (λ) of approximately 1.5 nm (17). Consequently, the influence of small amounts of surface contaminants on the analysis of a sample can be neglected.

TPS of the oxidic nickel catalyst shows an H_2S consumption during isothermal sulfidation at room temperature for all samples. Part of it is caused by sulfidation of the nickel surface oxide and part can be attributed to adsorption by the alumina. Although not clearly visible in the H_2S traces, slightly above room temperature an H_2S desorption occurs since no simultaneous H_2 consumption can be seen. This observation has been made for all alumina-supported systems and for bare alumina (9, 13, 24, 25). In the temperature region from 350 to 500 K, all catalysts show a major H_2S consumption. For the HTC 100 and 200 catalysts, no significant change in H_2 concentration is observed in this region, leading to the conclusion that sulfidation into the thermodynamically stable sulfide occurs through O–S exchange, as proposed by Arnoldy *et al.* (11). In this mechanism, sulfidation takes place by intermolecular proton transfer from the S to the O. The HTC 400 and 500 catalysts show H_2 consumption simultaneously with H_2S consumption. This H_2 consumption can be correlated to the removal of a reactive species like sulfur or oxygen.

In the temperature region from 500 up to 600 K, all TPS profiles show H_2 consumption and H_2S production in stoichiometric amounts, which indicates the hydrogenation of excess sulfur according to $S + H_2 \rightarrow H_2S$. Apparently, excess sulfur, which is chemisorbed on coordinatively unsaturated sites, is removed in the sulfidation mixture in this temperature regime. Quantitative TPS shows that the sulfur-to-nickel ratio at 623 K varies between 0.70 and 0.81, indicating that for all catalysts Ni_3S_2 is formed during sulfidation up to 623 K.

In the temperature region from 700 to 1000 K, all TPS profiles also show H_2 consumption and H_2S production in stoichiometric amounts, indicating the reduction of sulfided nickel species (Fig. 3). Since no significant H_2S consumption was observed above 1000 K, it is concluded that no significant amounts of nickel aluminates are present.

TPR of the oxidic catalyst precursors reveals typical properties of the catalysts. The profiles show a reduction peak over a wide temperature range from 400 up to 850 K (Fig. 1). Scheffer *et al.* (12) identified different nickel species in an alumina-supported catalyst, based on the temperature range in which the species were reduced:

- up to 600 K: reduction of bulk nickel oxide;
- 600 K to 1000 K: reduction of disperse nickel oxide interacting with the support;
- 1000 K to 1273 K: reduction of nickel aluminates.

For the HTC 400 and 500 catalysts the presence of small amounts of a bulk oxide, that is, poorly dispersed NiO, seem to be present, as can be inferred from the hydrogen consumptions peaking at 520–540 K. The broad reduction peak from 400 up to 850 K in the TPR profiles indicates the presence of a highly dispersed nickel oxide. In this hydrogen consumption two distinct contributions can be seen, the nature of which is not fully clear yet. Since for none of the catalysts a hydrogen consumption is observed in the temperature region from 1000 up to 1273 K, it is concluded that nickel aluminates are not present in the catalysts in significant amounts, in contrast to γ-Al_2O_3-supported nickel catalysts. This conclusion is supported by the TPS results discussed above. The absence of aluminates is an important feature of the studied catalysts since nickel aluminates are catalytically inactive for the reactions of interest (15, 16). It is suggested that the physical–chemical properties of the θ-Al_2O_3 surface are responsible for this special interaction between the nickel and the support (26). As it seems, the surface of θ-Al_2O_3, which is formed by heat treatment of γ-Al_2O_3, is less reactive, thus preventing the formation of Ni aluminate during the impregnation and/or calcination step. This suggestion is supported by Bolt *et al.* (27) who studied the formation of metal aluminate in transition metal oxides on γ-Al_2O_3 and α-Al_2O_3, which is formed by transition of γ-Al_2O_3 via θ-Al_2O_3 during heat treatment. It was concluded that the high grain boundary density of γ-Al_2O_3 is a major reason for its high reactivity toward aluminate formation, as compared to α-Al_2O_3. The "defect spinel structure" of γ-Al_2O_3 may also have a beneficial effect on the solid-state reaction between the nickel oxide and γ-Al_2O_3; it will facilitate cations to enter the alumina lattice. Apparently, the surface of θ-Al_2O_3 contains a sufficient number of optimized functional groups to bind the Ni particles, thus preventing sintering of the active phase during severe treatments. To accommodate the Ni oxide particles with (111) surface planes, the structure of the support should match the (111) plane. θ-Al_2O_3 has a monoclinic structure (28) and the (111) plane of oxygen is therefore likely to match the nickel oxide (111) plane. The slightly larger O–O distance of bulk nickel oxide (0.295 nm) or nickel hydroxide (0.312 nm), can be accommodated with minor strain effects and indicates a strong interaction with the support where the O–O distance is only 0.270 nm (2). Both the absence of aluminates and the presence of a highly dispersed nickel oxide/hydroxide clearly show the efficient use of the active nickel phase, making the catalysts industrially attractive.

TABLE 4

The Average Crystallite Size *c* in nm as Evaluated from the Quantitative XPS

	c (nm) Ox	*c* (nm) sulfided Ox	*c* (nm) RP	*c* (nm) sulfided RP
HTC 100	—	0.4	1.3	2.3
HTC 200	0.6	1.3	2.2	3.6
HTC 400	0.4	0.5	2.5	3.2
HTC 500	1.6	0.8	2.1	3.6

Using the model of Kerkhof and Moulijn (29), the (Ni 3*s*)/(Al 2*s*) emission line intensity ratio shown in Figs. 5 and 6 can be used to make an estimate of the crystallite size. Following this model, the linear correlation found at a metal loading up to about 8.0 wt% indicates an atomic dispersion in this regime. This linear correlation can be extrapolated to higher loading to normalize the observed (Ni 3*s*)/(Al 2*s*) ratios at a higher nickel loading. From this normalized intensity ratio, the average particle size can be evaluated. The calculated crystallite size for the oxidic, RP catalysts and their sulfided counterparts are collected in Table 4 and projected in Fig. 7.

As can be seen, for the oxidic catalysts the crystallite size varies from 0.4 to 1.6 nm. For the sulfided oxidic catalysts about the same crystallite size is found as for their oxidic counterparts. The small loss in dispersion can be attributed to the difference in the chemical composition. After reduction and passivation of the catalyst, the average crystallite size has increased to about 2.1–2.5 nm for all catalysts, except for the HTC 100 where the average size is only 1.3 nm. This observation stresses once more the special interaction between the active phase and the support which apparently results in a crystallite size which is essentially independent of the metal loading and preceding history of treatments for the catalysts under investigation. After sulfidation, the

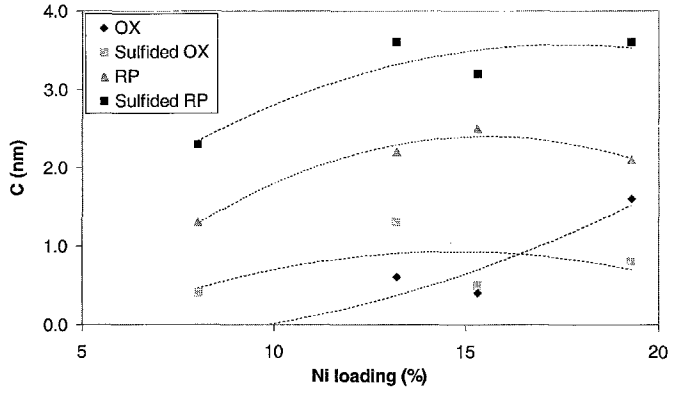

FIG. 7. Crystallite size of the HTC catalysts as a function of Ni loading as evaluated from the quantitative XPS.

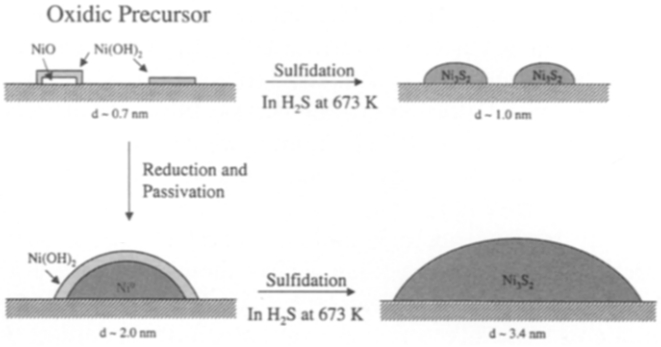

FIG. 8. Simplified models of nickel particles of the HTC catalysts.

average crystallite size of the RP catalysts slightly increases again, up to about 3.2–3.6 nm, except again for the HTC 100 catalyst, which has a crystallite size of ca. 2.3 nm. Figure 8 shows simplified models of the oxidic and RP nickel particles on the Al_2O_2 support. It is suggested that RP catalysts consist of a metallic nucleus and a hydroxide outer layer, in agreement with quantitative EXAFS analysis (2). The reason for the loss in dispersion upon sulfidation in H_2S/H_2 at 623 K for the RP catalysts is that besides O–S exchange (MeOx → MeS) also metallic nickel (Me → MeS) is sulfided. As a consequence, its density decreases and its crystallite size increases. Metallic Ni has a bulk density of 8.90 g ml^{-1}, whereas the produced Ni_3S_2 has a bulk density of 5.87 g ml^{-1} (30). From the ratio of densities, the ratio of volumes can be derived, leading to a ratio of the crystallite radii when the particles are assumed spherical. Calculations show that when a metallic nickel particle of 2.0 nm is sulfided, this will lead to a sulfidic particle of 3.7 nm, in good agreement with the obtained results collected in Table 4. Thus, the increase in particle size is caused by a change in chemical composition rather than by migration of the particles.

CONCLUSIONS

The oxidic catalysts contain a highly disperse nickel species, which consist of a hydroxide up to a nickel loading of about 13.2 wt% and of an oxidic core and a hydroxide outer layer for higher Ni loading. The crystallite size of the active phase varies between 0.4 and 1.6 nm. With TPR, an excess of oxygen (O/Ni = 1.2–1.5) is found. The RP catalysts consist of a metallic nucleus and a hydroxide outer layer. From quantitative XPS the crystallite size of the RP catalysts is estimated to be in the range of 1.3–2.5 nm. In contrast, the loss in surface area of the oxidic precursor after sulfidation is relatively small and can be attributed to the change in chemical composition rather than by sintering effects. Clearly, the reduction and passivation procedure results in a relatively larger loss of dispersion. Both TPR and

TPS show that no detectable amount of nickel aluminates are present, which can be attributed to the low reactivity of the θ-Al_2O_3 support as compared to γ-Al_2O_3.

After sulfidation up to 673 K, sulfur-to-nickel ratios between 0.70 and 0.81 are found, which corresponds to Ni_3S_2. Sulfidation of oxidic nickel catalysts takes place via O–S exchange.

Both the absence of aluminates and the presence of a highly disperse nickel oxide clearly show the efficient use of the active nickel phase and the θ-Al_2O_3 support, resulting in a crystallite size which is essentially independent of the metal loading and preceding history of treatments for the catalysts under investigation.

ACKNOWLEDGMENTS

The authors gratefully thank E. J. M. Fakkeldij for her assistance with the XPS data acquisition and R. Chandoesing and B. M. Vogelaar for their assistance in the temperature-programmed reactions. The research has been performed under auspices of NIOK, the Netherlands Institute for Catalysis Research, Lab Report TUD 00-4-1080.

REFERENCES

1. Janssens, J. P., van Langeveld, A. D., Bonné, R. L. C., Lok, C. M., and Moulijn, J. A., *in* "Hydrotreating Technology for Pollution Control," (M. Occelli and R. Chianelli, Eds.). p. 159. Marcel Dekker, New York, 1996.
2. Shido, T., Lok, M., and Prins, R., *Top. Catal.* **8**, 223 (1999).
3. Bourne, K. H., Holmes, P. P., and Pitkethly, R. C., *in* "Proceedings, 3rd International Congress on Catalysis, Amsterdam 1964" (W. M. H. Sachtler, G. C. A. Schuit, and P. Zwietering, Eds.), Vol. 2. Wiley, New York, 1965.
4. Poels, E. K., van Beek, W. P., Denhoed, W., and Visser, C., *Fuel* **74**, 1800 (1995).
5. Warburton, D. R., Wincott, P. L., Thornton, G., Quinn, F. M., and Norman, D., *Surf. Sci.* **211**, 71 (1989).
6. Harte, S. P., Vinton, S., Lindsay, R., Hakansson, L., Muryn, C. A., Thornton, G., Dhanak, V. R., Robinson, A. W., Binsted, N., Norman, D., and Fischer, D. A., *Surf. Sci.* **380**, L463 (1997).
7. Woodhead, A. P., Harte, S. P., Haycock, S. A., Muryn, C. A., Wincott, P. L., Dhanak, V. R., and Thornton, G., *Surf. Sci.* **420**, L138 (1999).
8. Yokoyama, T., Hamamatsu, H., Kitajima, Y., Takata, Y., Yagi, S., and Ohta, T., *Surf. Sci.* **313**, 197 (1994).
9. Mangnus, P. J., Poels, E. K., van Langeveld, A. D., and Moulijn, J. A., *J. Catal.* **137**, 92 (1992).
10. Den Besten, I. E., and Selwood, P. W., *J. Catal.* **1**, 93 (1962).
11. Arnoldy, P., van den Heijkant, J. A. M., de Bok, G. D., and Moulijn, J. A., *J. Catal.* **92**, 35 (1985).
12. Scheffer, B., Molhoek, P., and Moulijn, J. A., *Appl. Catal.* **46**, 11 (1989).
13. Arnoldy, P., and Moulijn, J. A., *J. Catal.* **93**, 38 (1985).
14. Mangnus, P. J., Bos, A., and Moulijn, J. A., *J. Catal.* **146**, 437 (1994).
15. Yasuda, H., Higo, M., Yoshitomi, S., Sato, T., Imamura, M., Matsubayashi, H., Shimada, H., Nishijima, A., and Yoshimura, Y., *Catal. Today* **39**, 77 (1997).
16. Salagre, P., Fierro, J. L. G., Medina, F., and Sueiras, J. E., *J. Mol. Catal. A—Chem.* **106**, 125 (1996).
17. Gijzeman, O. L. J., Debije Institute, University of Utrecht, The Netherlands.
18. Ng, K. T., and Hercules, D. M., *J. Phys. Chem.* **80**, 2094 (1976).
19. McIntyre, N. S., and Cook, M. G., *Anal. Chem.* **47**, 2208 (1975).
20. Kim, K. S., and Winograd, N., *Surf. Sci.* **43**, 625 (1974).
21. Kim, K. S., and Davis, R. E., *J. Electron Spectrosc. Relat. Phenom.* **1**, 251 (1973).
22. McIntyre, N. S., Rummery, T. E., Cook, M. G., and Owen, D., *J. Electrochem. Soc.* **123**, 1164 (1976).
23. Kim, K. S., Baitinger, W. E., Amy, J. W., and Winograd, N., *J. Electron Spectrosc. Relat. Phenom.* **5**, 351 (1974).
24. Mangnus, P. J., Poels, E. K., and Moulijn, J. A., *Ind. Eng. Chem. Res.* **32**, 1818 (1993).
25. Saur, O., Chevreau, T., Lamotte, J., Travert, J., and Lavalley, J.-C., *J. Chem. Soc. Faraday Trans. 1* **77**, 427 (1981).
26. Lindfors, L. P., and Smeds, S., *Catal. Lett.* **28**, 291 (1994).
27. Bolt, P. H., Habraken, F. H. P. M., and Geus, J. W., *J. Solid State Chem.* **135**, 59 (1998).
28. Pearson, W. B., Ed., *Struct. Rep.* **24**, 305 (1960).
29. Kerkhof, F. P. J. M., and Moulijn, J. A., *J. Phys. Chem.* **83**, 1612 (1979).
30. "Handbook of Chemistry and Physics," (D. R. Lide, Ed.), 76th ed. CRC Press, Boca Raton, FL, 1995–1996.